Half-metallic ferromagnetism and intrinsic anomalous Hall effect in the topological Heusler compound Co$_2$MnGe

Sudipta Chatterjee ⬡,*,† Saheli Samanta,* Barnali Ghosh, and Kalyan Mandal
Department of Condensed Matter and Materials Physics, S. N. Bose National Centre for Basic Sciences,
JD Block, Sector III, Salt Lake, Kolkata 700106, India

Half-metallic ferromagnets (HMFs) are ferromagnetic metallic compounds with 100% spin polarization at the Fermi level (E_F), and thus they are of particular interest in the field of spintronics, but the identification of HMFs with experiments is a challenging task. In principle, temperature-dependent electrical transport measurements should sensitively probe the half-metallic ferromagnetism since the spin-flip electron-magnon scattering mechanism is expected to be absent. In this work, we perform a systematic temperature-dependent electrical transport measurement on the ferromagnetic full Heusler compound Co$_2$MnGe. Our experimental results reveal that Co$_2$MnGe exhibits an exponential suppression of spin-flip electron-magnon scattering below a characteristic crossover temperature ($\Delta \sim 79$ K), which suggests that this material possesses a perfect spin polarization at the low temperature. The energy gap ($k_B\Delta$) characterizing the suppression of spin-flip electron-magnon scattering is $\sim$7 meV. This key finding is further established by a sign change in magnetoresistance at $T \gtrsim \Delta$. Moreover, we have also studied the anomalous Hall effect (AHE) of the present compound. We find a notable change in the ordinary Hall coefficient (R_0) and in the carrier density (n) at $T \lesssim \Delta$, which is consistent with the complete absence of minority-spin states at the E_F. The anomalous Hall resistivity (ρ_{yx}^A) is observed to scale near quadratically with the longitudinal resistivity (ρ_{xx}), and further experimental analysis indicates that the AHE in Co$_2$MnGe is dominated by the intrinsic Karplus-Luttinger Berry phase mechanism. These findings imply that the Co$_2$MnGe is a rare ferromagnetic full Heusler compound in which half-metallicity coexists with the topology-driven AHE.

I. INTRODUCTION

Spin-dependent electrical transport has been a topic of renewed interest since the discovery of giant magnetoresistance (GMR) in 1988 [1,2], especially due to its potential technological applications. Half-metallic ferromagnets (HMFs) are a class of magnetic materials characterized by the coexistence of metallic nature for one electron spin and insulating nature for the other [3]. Thus, they possess 100% spin polarization at the Fermi level (E_F). Figure 1(a) represents a schematic of the density of states (DOS) of an HMF for the minority and majority electrons. Due to the complete absence of minority-spin states at the E_F, an energy gap $k_B\Delta$ arises for only one spin direction and, hence, it shows various consequences in transport properties [4]. The presence of an energy gap suppresses the spin-flip electron-magnon scattering of the conduction electrons and, therefore, the electrical resistivity (ρ) exhibits an exponential suppression of the T^2 dependence [5–9]. In spite of its simplicity, the experimental realization of half-metallic ferromagnetism is still very challenging [10,11].

In general, the HMFs are theoretically recognized by the band structure and the integer spin moments calculation [12], while surface-sensitive experimental techniques such as spin-resolved photoemission spectroscopy [13,14], scanning

tunneling microscopy [15], and point-contact Andreev reflection measurements [16,17] are utilized to identify an HMF. However, temperature-dependent electrical resistivity and magnetoresistance (MR) are the bulk measurements and can, in principle, precisely identify a true HMF because of the absence of spin-flip electron-magnon scattering at the E_F. There are numerous theories for spin-flip electron magnon scattering in HMFs [7,10,18,19], which has been extensively implemented for the identification of HMFs, for instance, in CrO$_2$ [8,10,11,20], perovskite manganites [14,21,22], and Heusler alloys [7,23,24]. In the context of Heusler alloys, the concept of HMF was first introduced by de Groot *et al.* in NiMnSb [3]. Half-metallic ferromagnetism has also been predicted theoretically for many other Heusler compounds [25–31], but apart from the pioneering studies on Co$_2$FeSi [7] and Co$_2$MnSi [24,32,33], the experimental understanding of actual HMF materials among Heusler compounds is still very elusive.

In the family of Heusler compounds, Co$_2$-based ferromagnetic full Heusler compounds with cubic $L2_1$ structures have a unique position in the hierarchy of half-metals because of their high Curie temperatures, which are important for the application of half-metals at finite temperatures [34]. Due to their highly tunable electronic and magnetic properties [35–37], various novel topological transport and magneto-transport phenomena are also observed in these compounds, like the anomalous Hall effect (AHE), the anomalous Nernst effect, the chiral anomaly, etc. [38–45]. Among these various Co$_2$-based full Heusler compounds, Co$_2$MnGe has been

*These authors contributed equally to this work.
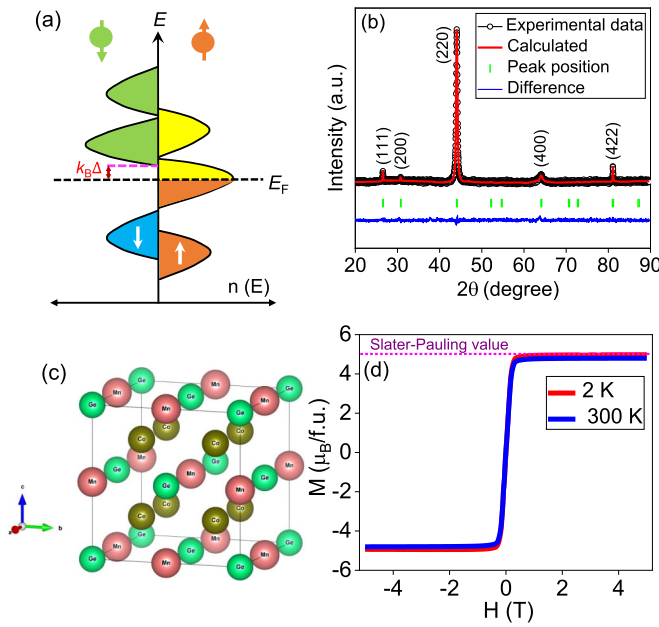†schatterjee@bose.res.in

FIG. 1. (a) Schematic representation of the density of states (DOS) of a half-metallic ferromagnet for the majority and minority electrons with an energy gap ($k_B\Delta$) at the Fermi level (E_F) for minority electrons. (b) The Rietveld refinements at room temperature of the XRD pattern for Co_2MnGe. The experimental data are represented by the black circles, and the calculated result is shown by the solid red line. The vertical green lines represent the Bragg peak positions, whereas the solid blue line at the bottom represents the difference between experimental and calculated data. (c) The corresponding crystal structure of Co_2MnGe. (d) Field-dependent magnetization curves up to 5 T at 2 and 300 K. The Slater-Pauling value of magnetization is marked by a dotted magenta line.

theoretically predicted to exhibit 100% spin polarization at the E_F with a minority-spin gap of ~ 0.5 eV [46,47]. Co_2MnGe also possesses one of the highest Curie temperatures (~ 915 K) among the Heusler compounds [48]. Additionally, some of these Co_2-based magnetic full Heusler compounds have also been predicted to host the topological nontrivial state in their band structure [49,50]. Moreover, attempts to investigate anomalous transport properties in Co_2MnGe have yielded conflicting results regarding the origin of AHE [51,52]. Hence, Co_2MnGe provides a perfect platform for the experimental realization of half-metallic ferromagnetism and anomalous transport phenomena at the same time.

In this paper, we have systematically investigated the temperature-dependent electrical transport properties, i.e., resistivity, MR, and AHE, in the ferromagnetic full Heusler compound Co_2MnGe. Our experimental results reveal that the material under scrutiny, i.e., Co_2MnGe, is a true HMF at low temperatures because we indeed observe an exponential suppression of T^2 behavior in the electrical resistivity at $T \lesssim \Delta$, where $\Delta \sim 79$ K. This key finding is further supported by a sign change in the MR at $T \gtrsim \Delta$. Moreover, we have also investigated the AHE in Co_2MnGe and found an anomalous Hall conductivity (AHC) of ~ 140 S/cm at room temperature with an intrinsic contribution of ~ 118 S/cm. The calculated ordinary Hall coefficient (R_0) and carrier density (n)

exhibit significant changes at $T \lesssim \Delta$. Further experimental results suggest that the Berry phase-driven intrinsic Karplus-Luttinger (KL) mechanism is responsible for the observed AHE in Co_2MnGe.

The rest of the paper is organized as follows: In Sec. II, we detail the experimental methodologies utilized for the measurements. The experimental findings and analysis are discussed in Sec. III. Finally, the conclusions are drawn in Sec. IV.

II. EXPERIMENTAL DETAILS

Bulk polycrystalline Co_2MnGe was synthesized by a conventional arc-melting furnace under a high-purity argon atmosphere using high-purity of Co (~ 99.99%), Mn (~ 99.99%), and Ge (~ 99.99%) elements. The sample was remelted seven to eight times to ensure homogeneous melting. The as-cast ingot was then sealed in a vacuumed quartz tube, annealed at 1273 K for seven days, and then quenched in cold water. The structure and phase purity of the bulk Co_2MnGe were characterized by the x-ray diffraction (XRD) technique (Rigaku SmartLab) with Cu K_α radiation. Rietveld refinements for the experimentally obtained XRD data were performed using the "FULLPROF" software. The actual composition of the studied sample was confirmed by energy dispersive x-ray (EDX) analysis. Results are discussed in Sec. S1 of the Supplemental Material [53]. The magnetization measurements were carried out by using a vibrating sample magnetometer (VSM) in a physical property measurement system (PPMS, Quantum Design, USA). The sample used for the magnetic measurements was of approximate dimensions $0.4 \times 0.5 \times 4$ mm^3. For each $M(H)$ isotherm, we have stabilized the temperature at least for 30 min to achieve good thermal stability. The electrical and magnetic transport measurements were carried out using a physical property measurement system (PPMS, Quantum Design, USA) using the electrical transport option (ETO). Both the longitudinal and Hall resistivity measurements were performed in a standard four-probe method using conducting silver epoxy and copper wires. For the Hall resistivity (ρ_{yx}) measurements, to cancel out the longitudinal resistivity (ρ_{xx}) contribution due to the voltage probe misalignment, the final Hall resistivity was calculated by the difference of transverse resistance measured at the positive and negative fields.

III. RESULTS AND DISCUSSIONS

A. Structural and magnetization properties

To evaluate the crystal structure and the phase purity of the studied compound, we have taken room-temperature (~ 300 K) XRD data. Figure 1(b) depicts the room-temperature XRD pattern of the polycrystalline Co_2MnGe along with its Rietveld refinement. The corresponding crystal structure of the compound is represented in Fig. 1(c). The crystallographic positions of the Co atoms are $(0, 0, 0)$ and $(\frac{1}{2}, \frac{1}{2}, \frac{1}{2})$, while the Mn and Ge atoms are $(\frac{1}{4}, \frac{1}{4}, \frac{1}{4})$ and $(\frac{3}{4}, \frac{3}{4}, \frac{3}{4})$, respectively. The obtained XRD pattern shows no impurity peaks, and the Rietveld refinement of the XRD data ensures the single-phase nature of the present compound and its crystallization in the cubic $L2_1$ structure with the space
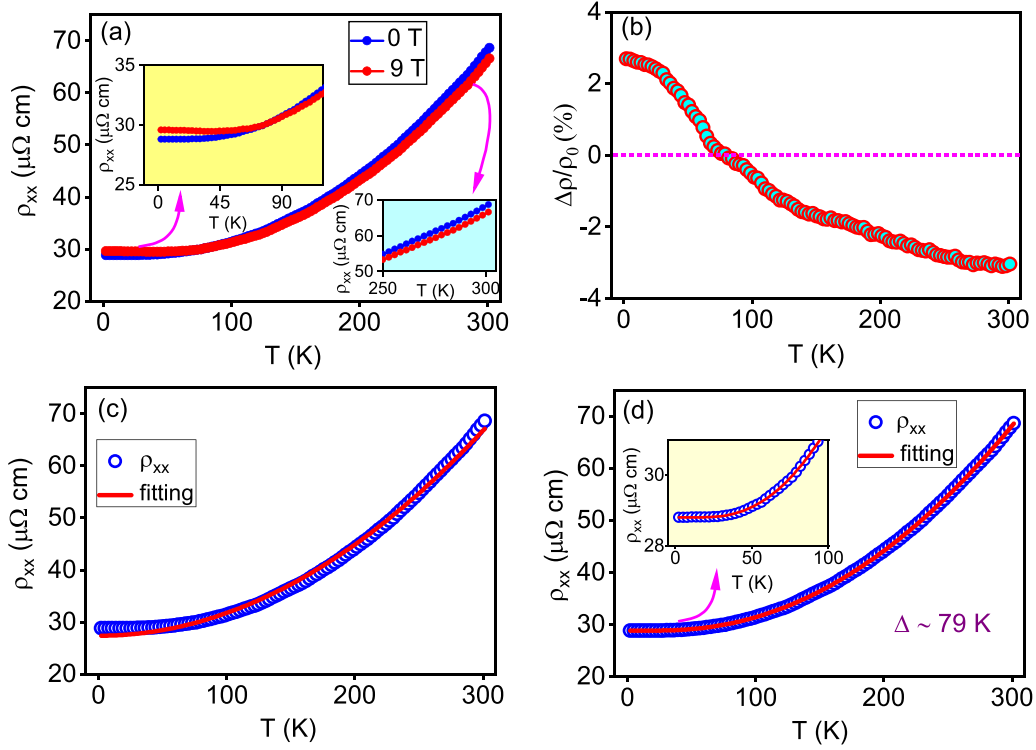
FIG. 2. (a) Temperature-dependent longitudinal resistivity (ρ_{xx}) for 0- and 9-T magnetic fields. The upper left inset shows the expanded view at low temperatures and the lower right inset represents the expanded view at high temperatures. (b) Temperature dependence of magnetoresistance (MR) at 9 T. (c) ρ_{xx} as a function of temperature at 0 T. The solid red line shows the fitting of Eq. (3) for a conventional ferromagnet. (d) The temperature variation of ρ_{xx} at 0 T along with the fitting of Eq. (5). The fitted curve is shown in red color. The inset shows an enlarged view of the fitting at low temperatures.

group $Fm\bar{3}m$. Generally, the ordered structure of Co$_2$-based full Heusler alloys marks the presence of both (111) and (200) superlattice reflections [43,54]. The presence of both (111) and (200) peaks suggests the ordered $L2_1$ structure of Co$_2$MnGe. The lattice parameter obtained from the refinement is found to be 5.748 Å, which is in good agreement with earlier reports [47,55].

The magnetic field-dependent dc magnetization at 2 and 300 K is shown in Fig. 1(d). It is noteworthy that the half-metallic full Heusler compounds generally follow the Slater-Pauling (SP) type behavior of magnetization [25]: $M_{tot} = (Z_{tot} - 24)\,\mu_B/\text{f.u.}$, where M_{tot} is the total magnetic moment and Z_{tot} is the total number of valence electrons in the unit cell of the compound. For Co$_2$MnGe, the value of Z_{tot} is 29. So, according to the above-mentioned relation, the total magnetic moment should be 5 $\mu_B/\text{f.u.}$ From Fig. 1(d), the value of saturation magnetization (M_S) is estimated to be around 4.98 $\mu_B/\text{f.u.}$ at 2 K, which is consistent with the SP rule. Because of the high Curie temperature of the material [48], the temperature dependence of the M_S is negligible up to room temperature.

B. Longitudinal resistivity and magnetoresistance

The temperature-dependent longitudinal resistivity (ρ_{xx}) for 0 and 9 T is demonstrated in Fig. 2(a). At 2 K, the residual resistivity value is estimated to be around 29 $\mu\Omega$ cm, which gives a residual resistivity ratio [RRR = $\rho_{xx}(300\,\text{K})/\rho_{xx}(2\,\text{K})$] ~ 2.4. This value is larger than most of the earlier reported val-

ues in Co$_2$-based full Heusler compounds [40,41,54,56–58], which indicates a comparatively clean sample. Usually, for a metallic ferromagnet, the electrical resistivity arises due to the scattering of conduction electrons from defects (ρ_0), magnons (ρ_M), and phonons (ρ_{ph}). According to Matthiessen's rule, the total electrical resistivity of ferromagnetic materials is attributed to the sum of all contributing scattering mechanisms [59,60]:

$$\rho_{xx}(T) = \rho_0 + \rho_{ph}(T) + \rho_M(T), \quad (1)$$

where residual resistivity ρ_0 is independent of temperature and the phononic contribution (ρ_{ph}) in the ρ_{xx} can be described with the Bloch-Grüneisen formula [7]

$$\rho_{ph}(T) = A\left(\frac{T}{\Theta_D}\right)^5 \int_0^{\Theta_D/T} \frac{x^5}{(e^x - 1)(1 - e^{-x})}dx, \quad (2)$$

where A is related to the strength of the electron-phonon scattering process. The magnonic term $\rho_M \propto T^2$ for spin-flip electron-magnon scattering in conventional ferromagnets, which gets exponentially suppressed in half-metallic ferromagnets. Now, considering Co$_2$MnGe to be a conventional ferromagnet, we have fitted the temperature-dependent ρ_{xx} data with the following equation [61]:

$$\rho_{xx}(T) = \rho_0 + \rho_{ph}(T) + \alpha T^2, \quad (3)$$

where αT^2 is the electron-magnon scattering term. The fitted curve with Eq. (3) is illustrated in Fig. 2(c). The fit quality is poor, as evidenced by the wide disparity between

the experimental and fitted data. Hence, Co_2MnGe cannot be considered as a conventional metallic ferromagnet and calls for the search for other unconventional scattering mechanisms. It is also noteworthy that the contributions due to the electron-phonon scattering are comparatively low ($A \sim 3.7 \times 10^{-10}$); therefore, the resistivity is mainly dominated by the ρ_M in this compound. All the fitting parameters are tabulated in Table S2 of the Supplemental Material [53].

In order to explain the unusual nature of the observed temperature-dependent resistivity, the predicted half-metallic character of the compound is taken into account. For an HMF, the minority-spin electronic states are completely gapped, while the majority-spin electronic states are gapless at the E_F. Thereby, the T^2 dependence of the spin-flip electron-magnon scattering is expected to be exponentially suppressed and is expressed by the empirical expression [7,10,60]

$$\rho_M = \beta T^2 \exp(-\Delta/T), \quad (4)$$

where the parameter β is related to the strength of the electron-magnon scattering process, and $k_B\Delta$ is the energy gap between the nearest band edge of unoccupied minority spins and the E_F. Now, the temperature-dependent zero-field longitudinal resistivity data are fitted with the relation, which is given as

$$\rho_{xx} = \rho_0 + \rho_{ph}(T) + \beta T^2 \exp(-\Delta/T). \quad (5)$$

It is evident from Fig. 2(d) that considering the exponential suppression of the T^2 dependence in the ρ_{xx} data significantly improved the fit quality. It reduced the chi-square value by more than an order of magnitude (see Table S2 of the Supplemental Material [53]). The enlarged view of the fitting is also shown in the inset of Fig. 2(d). The fitting gives $\Delta \sim 79$ K, which yields an energy gap ($k_B\Delta \sim 7$ meV). The exponential suppression of the T^2 term clearly signifies the existence of half-metallic ferromagnetism in Co_2MnGe, and it exists only for $T < \Delta$. However, the obtained energy gap is much smaller as compared to the theoretically predicted value [46,47]. A similar deviation of an energy gap in the experimental and theoretical values has also been observed previously in other HMFs [7,60]. It is also noteworthy that the experimentally observed energy gap in the studied compound Co_2MnGe (~ 7 meV) is smaller than that of the Co_2FeSi (~ 9 meV) [7], despite the fact that Mn has one fewer d electron than Fe, which should place the Fermi surface even further from the bottom of the minority-spin band. This difference in the observed energy gap results from a substantial change in the binding energy between Si and Ge [46]. Interestingly, theoretical investigations reveal that the half-metallic energy gap is smaller in Co_2MnGe (~ 0.54 eV) [46] than in Co_2FeSi (~ 0.655 eV) [62], which is in accordance with our experimental findings.

Another independent verification of half-metallicity can be obtained from the corresponding MR measurements of Co_2MnGe. The temperature dependence of MR can be measured by using the following equation:

$$MR = \left[\frac{\rho_{xx}(H) - \rho_{xx}(0)}{\rho_{xx}(0)} \right] \times 100\% = \frac{\Delta\rho}{\rho_0} \times 100\%, \quad (6)$$
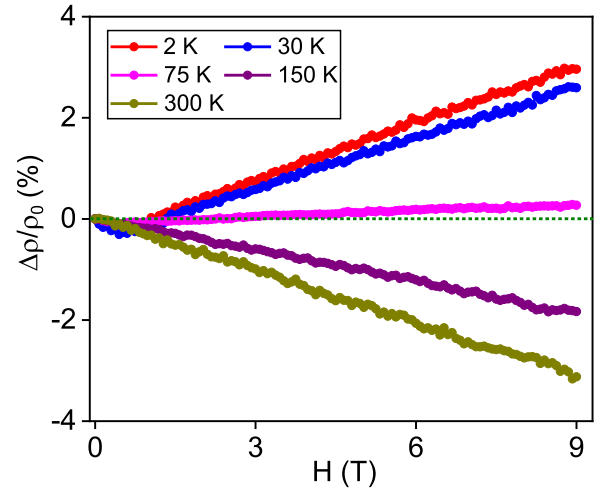

FIG. 3. Magnetic field dependence of the magnetoresistance (MR) at different temperatures.

where $\rho_{xx}(H)$ and $\rho_{xx}(0)$ are the electrical resistivity under H and zero field, shown in Fig. 2(a). A maximum MR value of $\sim 3\%$ is observed under an applied field of 9 T. It can be clearly seen from Fig. 2(b) that $\frac{\Delta\rho}{\rho_0} > 0$ when $T \lesssim 79$ K, and $\frac{\Delta\rho}{\rho_0} < 0$ when $T \gtrsim 79$ K.

Further, to get more insight about the crossover in $\frac{\Delta\rho}{\rho_0}$ we measured the field-dependent resistivity at various constant temperatures as shown in Fig. 3. At higher magnetic fields, the resistivity increases with the increasing field at low temperatures and decreases with the increasing field at higher temperatures. The observed temperature dependence of MR can be explained by the above-mentioned scenario, where the resistivity is dominated by the gapped spin-flip electron-magnon scattering. The low-temperature MR remains negative for conventional ferromagnets, whereas, in HMFs, due to the complete absence of minority-spin states at the E_F, spin-flip scattering is exponentially suppressed for $T < \Delta$ and the MR crosses over from a negative to a positive value on decreasing temperature [7]. Indeed, such behavior is observed in both Figs. 2(b) and 3 at $T \gtrsim 79$ K.

C. Anomalous Hall effect

After proving Co_2MnGe as an HMF for $T \lesssim \Delta$, we have studied the AHE in a wide temperature range from 2 to 300 K in this compound. Figure 4(a) represents the magnetic field dependence of Hall resistivity (ρ_{yx}) at different constant temperatures. The schematic diagram of the sample device used for the longitudinal voltage (V_x) and Hall voltage (V_y) measurements is shown in the right inset of Fig. 4(a). At a low field, the $\rho_{yx}(H)$ increases sharply with an increase in the field, and it changes its slope close to the saturation field (~ 0.5 T), whereas, in the high-field region, the $\rho_{yx}(H)$ exhibits a weak linear field dependence up to 9 T. The isothermal field dependence of dc magnetization is shown in Sec. S2 of the Supplemental Material [53] at various constant temperatures. The identical nature of the shapes of $\rho_{yx}(H)$ and $M(H)$ curves in the low-field region confirms the presence of AHE in Co_2MnGe.
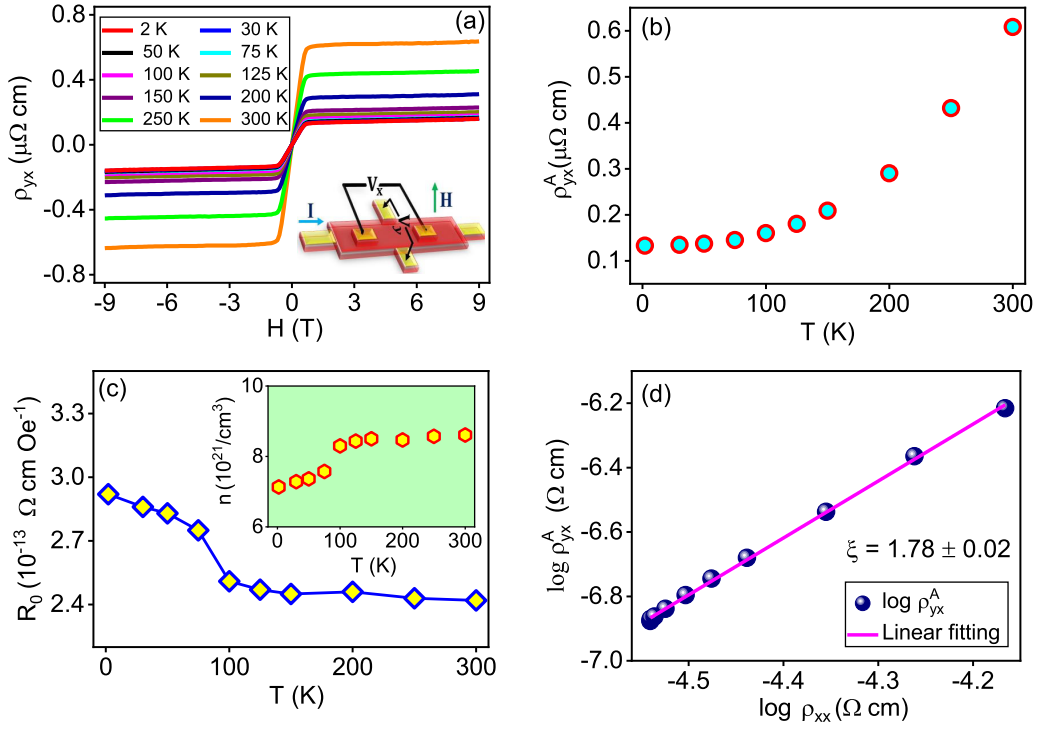
FIG. 4. (a) Magnetic field-dependent Hall resistivity (ρ_{yx}) at different temperatures from 2 to 300 K. The right inset shows the sample device used for the longitudinal and Hall resistivity measurements. (b) Temperature dependence of anomalous Hall resistivity (ρ_{yx}^A). (c) Temperature dependence of the ordinary Hall coefficient (R_0). Inset shows the temperature-dependent carrier density n. (d) Double-logarithmic plot between ρ_{yx}^A and ρ_{xx} and the linear fitting is shown in the magenta line.

In general, the Hall resistivity ρ_{yx} for ferromagnets is made up of two components [63],

$$\rho_{yx} = \rho_{yx}^0 + \rho_{yx}^A = R_0 H + R_S \mu_0 M, \qquad (7)$$

where R_0 and R_S are the ordinary and anomalous Hall co-efficients, and μ_0 is the vacuum permeability. The first term (ρ_{yx}^0) is the ordinary Hall resistivity that arises from the triv-ial Lorentz force, and the second term (ρ_{yx}^A) represents the anomalous Hall contribution that originates from intrinsic magnetization, respectively. The ρ_{yx}^A and R_0 can be obtained from the linear fit of $\rho_{yx}(H)$ at the high-field region. The y-axis intercept and the slope of the linear fit correspond to ρ_{yx}^A and R_0, respectively. The R_S can be calculated by using the relation $\rho_{yx}^A = R_S \mu_0 M_s$. In Fig. 4(b), anomalous Hall resistivity ρ_{yx}^A is depicted as a function of temperature; from 2 to 300 K, it increases monotonically. Figure 4(c) represents the temperature dependence of R_0. The positive values of R_0 indicate that the transport properties in Co_2MnGe are mainly dominated by hole-type charge carriers in the whole tem-perature range. Using the formula $R_0 = 1/ne$, one can also determine the temperature-dependent carrier density (n) and carrier type. Using the values of R_0, the carrier density n is obtained, as depicted in the inset of Fig. 4(c). It can be clearly seen from Fig. 4(c) that there is a considerable change in R_0 and n at $T \lesssim \Delta$ because of the absence of minority density of states at the E_F [5]. The estimated carrier density at 2 K is $\sim 7.13 \times 10^{21}$ cm^{-3}, and the associated carrier mobility (μ_h) is ~ 30 cm^2 V^{-1} S^{-1}. The temperature variation of R_S is

depicted in Fig. S3 of the Supplemental Material [53]; similar to ρ_{yx}^A, it also increases monotonically as the temperature rises.

Further, to investigate the origin of AHE in Co_2MnGe, we have checked the scaling behavior of ρ_{yx}^A according to the scaling relation $\rho_{xy}^A \propto \rho_{xx}^\xi$ [63], in the temperature range 2 to 300 K on a double-logarithm scale. Generally, the AHE in metallic ferromagnets originates either from the intrinsic Karplus-Luttinger (KL) mechanism [64] which has been re-cently explained by the Berry phase effect of the occupied electronic Bloch states [65,66] or by an extrinsic mechanism (i.e., side jump or skew scattering), which can be under-stood as a result of asymmetric scattering from the spin-orbit interaction acting on the conduction electrons or impurities [67,68]. While for skew scattering the ρ_{yx}^A is linearly pro-portional to ρ_{xx} (i.e., $\xi \approx 1$), on the other hand, side-jump scattering is proportional to ρ_{xx}^2 (i.e., $\xi \approx 2$), similar to that of the intrinsic KL mechanism [63]. In Fig. 4(d), a linear fitting is employed to determine the exponent ξ accord-ing to the aforementioned scaling relation. We determined the exponent ξ be ~ 1.78, which suggests that the AHE in Co_2MnGe is dominated by intrinsic Karplus-Luttinger (KL) or extrinsic side-jump mechanisms. It has been shown that the extrinsic side-jump contribution of AHC is on the order of $[e^2/(ha)(\epsilon_{SO}/E_F)]$, where ϵ_{SO} is the spin-orbit interaction and E_F is the Fermi energy [69,70]. The terms e, h, and a denote the electronic charge, Planck constant, and lattice parameter, respectively. The term (ϵ_{SO}/E_F) is typically on the order of 10^{-2} for most of the metallic ferromagnets [41,54,58].
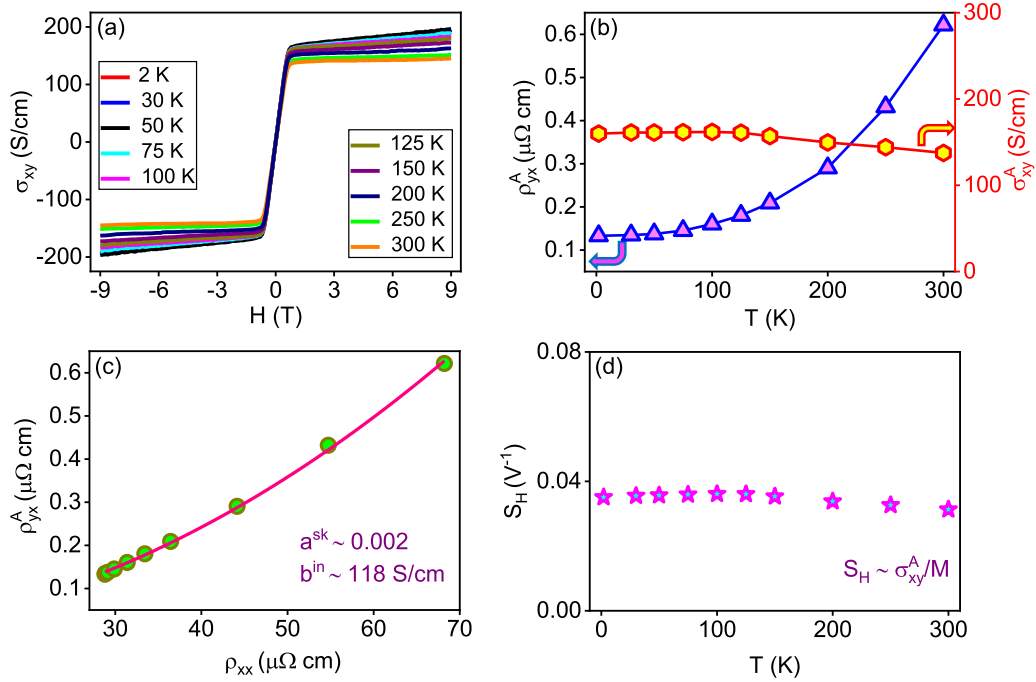
FIG. 5. (a) Magnetic field-dependent Hall conductivity (σ_{xy}) at different temperatures. (b) Temperature dependence of anomalous Hall resistivity (ρ_{yx}^A) and anomalous Hall conductivity (σ_{xy}^A). (c) Plot of ρ_{yx}^A vs ρ_{xx}. The fitted curve is shown in a solid pink color. (d) Temperature dependence of the scaling coefficient (S_H).

Therefore, as compared to intrinsic AHC, the contribution from extrinsic side jump should be very small. Hence, the intrinsic Berry phase-driven KL mechanism dominates the AHE in Co$_2$MnGe.

In order to comprehend the microscopic origin of the observed AHE in the studied compound, we need to look at the variation of AHC with ρ_{yx}^A and temperature. Therefore, using the following conversion relation [39,58], we have calculated the Hall conductivity (σ_{xy}):

$$\sigma_{xy} = \frac{\rho_{yx}}{\left(\rho_{yx}^2 + \rho_{xx}^2\right)}. \tag{8}$$

The magnetic field-dependent Hall conductivity data at various temperatures are depicted in Fig. 5(a). Using zero-field extrapolation of high-field Hall conductivity data along the y axis, we have extracted the AHC (σ_{xy}^A). Temperature-dependent σ_{xy}^A and ρ_{yx}^A are plotted in Fig. 5(b), and the change of AHC is almost temperature independent, illustrating that the origin of AHE in Co$_2$MnGe is intrinsic in nature [58,71]. At 2 K, the value of AHC is $\sim$160 S/cm and does not change largely up to room temperature ($\sim$140 S/cm). The observed AHC in Co$_2$MnGe is comparable to that reported for several ferromagnetic Heusler compounds [38,41,43,54]. It is worth noting here that the intrinsic AHE is likely to dominate in the overall behavior of the AHE when the sample's longitudinal conductivity (σ_{xx}) is in the good metallic range, i.e., σ_{xx} is of the order of $10^4 - 10^6$ S/cm [63]. The temperature-dependent σ_{xx} is shown in Sec. S4 of the Supplemental Material [53]. For the present system, the σ_{xx} is found to be $\sim 3.5 \times 10^4$ S/cm and 1.5×10^4 S/cm at 2 and 300 K, respectively. These values lie under the category of a good metallic regime, in which

the AHE is primarily attributed to the intrinsic Berry-phase mechanism.

To differentiate the intrinsic and extrinsic components of AHC, we plotted the ρ_{yx}^A with the ρ_{xx} as illustrated in Fig. 5(c) and fitted it using the equation [43,58]

$$\rho_{yx}^A = a^{sk}\rho_{xx} + b^{in}\rho_{xx}^2, \tag{9}$$

where a^{sk} is the skew-scattering coefficient and b^{in} is the Berry phase-driven intrinsic AHC, respectively. We found a^{sk} to be $\sim$0.002 and intrinsic AHC, b^{in} to be $\sim$118 S/cm. Therefore, the intrinsic Berry phase-driven mechanism is responsible for more than 84% of the total AHC at 300 K in Co$_2$MnGe. As the intrinsic AHC is nearly proportional to the magnetization, the scaling coefficient ($S_H = \frac{R_S\mu_0}{\rho_{xx}^2} = \frac{\sigma_{xy}^A}{M}$) should be constant and temperature independent [41,54,72]. Figure 5(d) demonstrates that S_H is nearly independent of temperature, confirming further the dominant intrinsic Berry phase contribution to the AHE in Co$_2$MnGe. The calculated S_H value is comparable to that reported in the literature for numerous Heusler compounds and ferromagnetic systems ($S_H \sim 0.01$–0.2 V^{-1}) [41,54,73].

Furthermore, it is important to note that Obaida et al. showed that the AHE came from an extrinsic skew-scattering mechanism in Co$_2$MnGe thin film [51], where the RRR value (<1) is considerably lower than that reported in this work. On the contrary, recent theoretical investigations [50] and the angle-resolved photoelectron spectroscopy (ARPES) experiment [52] on bulk Co$_2$MnGe reveal that this compound exhibits time-reversal symmetry-breaking topological Weyl fermions in its electronic band structure, where one can anticipate a large Berry phase-driven intrinsic AHE, which is consistent with our experimental findings of Berry

phase-driven intrinsic AHE in Co_2MnGe. The experimentally determined AHC ($\sim$140 S/cm at 300 K) is also comparable to the value predicted theoretically [50].

While Berry phase-driven intrinsic AHE has been seen in a number of topological Heusler compounds in the past [39,41,43,58], true half-metallic ferromagnetism along with intrinsic AHE (this study) is rather scarce in topological Heusler compounds. For example, the ferromagnetic full Heusler compounds such as Co_2MnGa and Co_2MnAl display a very large intrinsic AHC but do not exhibit true half-metallicity [39,42]. Similarly, the topological Heusler compounds Co_2TiZ (where $Z = Si$, Ge, and Sn) also show Berry phase-driven AHE, but do not exhibit true half-metallic ferromagnetism [40,41]. On that account, Co_2MnGe is a very rare ferromagnetic Heusler compound where the half-metallicity coexists with a topologically nontrivial band structure at low temperatures.

IV. CONCLUSIONS

In summary, our magnetic, transport, and magnetotransport measurements yield significant evidence that Co_2MnGe is a true HMF at $T \lesssim \Delta$ (where $\Delta \sim 79$ K) because we indeed observe an exponential suppression of spin-flip electron-magnon scattering at $T \lesssim \Delta$. The claim is further supported by a sign change in MR from positive at low temperatures ($T \lesssim \Delta$) to negative at higher temperatures. Nevertheless, the obtained half-metallic gap $k_B\Delta \sim 7$ meV is significantly

smaller than the theoretically predicted value. Moreover, we have also investigated the AHE in the present compound. The ordinary Hall coefficient and carrier density show notable changes at $T \lesssim \Delta$ due to the absence of minority-spin states at the E_F. We find an AHC of $\sim$140 S/cm at room temperature with an intrinsic contribution of $\sim$118 S/cm, which is comparable with the theoretically predicted value. The ρ_{yx}^A scales near quadratically with the ρ_{xx}, and our detailed experimental analysis demonstrates that in AHC, the Berry phase-driven intrinsic KL mechanism dominates over the extrinsic mechanisms in Co_2MnGe. The coexistence of half-metallic ferromagnetism and topology-driven AHE is very rare in magnetic Heusler compounds. Thus, this work provides a suitable platform for future studies of half-metallic ferromagnetism along with Berry phase-driven AHE in other topological Heusler compounds.

[1] M. N. Baibich, J. M. Broto, A. Fert, F. Nguyen Van Dau, F. Petroff, P. Etienne, G. Creuzet, A. Friederich, and J. Chazelas, Phys. Rev. Lett. **61**, 2472 (1988).

[2] I. Žutić, J. Fabian, and S. Das Sarma, Rev. Mod. Phys. **76**, 323 (2004).

[3] R. A. de Groot, F. M. Mueller, P. G. van Engen, and K. H. J. Buschow, Phys. Rev. Lett. **50**, 2024 (1983).

[4] M. I. Katsnelson, V. Y. Irkhin, L. Chioncel, A. I. Lichtenstein, and R. A. de Groot, Rev. Mod. Phys. **80**, 315 (2008).

[5] J. Moodera and D. Mootoo, J. Appl. Phys. **76**, 6101 (1994).

[6] X. Wang and X.-G. Zhang, Phys. Rev. Lett. **82**, 4276 (1999).

[7] D. Bombor, C. G. F. Blum, O. Volkonskiy, S. Rodan, S. Wurmehl, C. Hess, and B. Büchner, Phys. Rev. Lett. **110**, 066601 (2013).

[8] M. S. Anwar and J. Aarts, Phys. Rev. B **88**, 085123 (2013).

[9] S. M. Watts, S. Wirth, S. von Molnár, A. Barry, and J. M. D. Coey, Phys. Rev. B **61**, 9621 (2000).

[10] A. Barry, J. M. D. Coey, L. Ranno, and K. Ounadjela, J. Appl. Phys. **83**, 7166 (1998).

[11] J. M. D. Coey and M. Venkatesan, J. Appl. Phys. **91**, 8345 (2002).

[12] J. Coey and C. Chien, MRS Bull. **28**, 720 (2003).

[13] K. P. Kämper, W. Schmitt, G. Güntherodt, R. J. Gambino, and R. Ruf, Phys. Rev. Lett. **59**, 2788 (1987).

[14] J.-H. Park, E. Vescovo, H.-J. Kim, C. Kwon, R. Ramesh, and T. Venkatesan, Nature (London) **392**, 794 (1998).

[15] V. Y. Irkhin and M. I. Katsnelson, Phys. Rev. B **73**, 104429 (2006).

[16] R. J. Soulen, J. M. Byers, M. S. Osofsky, B. Nadgorny, T. Ambrose, S. F. Cheng, P. R. Broussard, C. T. Tanaka, J. Nowak, J. S. Moodera, A. Barry, and J. M. D. Coey, Science **282**, 85 (1998).

[17] Y. Ji, G. J. Strijkers, F. Y. Yang, C. L. Chien, J. M. Byers, A. Anguelouch, G. Xiao, and A. Gupta, Phys. Rev. Lett. **86**, 5585 (2001).

[18] A. Gupta, X. Li, and G. Xiao, J. Appl. Phys. **87**, 6073 (2000).

[19] N. Furukawa, Y. Shimomura, T. Akimoto, and Y. Moritomo, J. Magn. Magn. Mater. **226-230**, 782 (2001).

[20] K. Suzuki and P. M. Tedrow, Phys. Rev. B **58**, 11597 (1998).

[21] M. Jaime, P. Lin, M. B. Salamon, and P. D. Han, Phys. Rev. B **58**, R5901 (1998).

[22] T. Akimoto, Y. Moritomo, A. Nakamura, and N. Furukawa, Phys. Rev. Lett. **85**, 3914 (2000).

[23] J. C. Prestigiacomo, D. P. Young, P. W. Adams, and S. Stadler, J. Appl. Phys. **115**, 043712 (2014).

[24] M. Jourdan, J. Minár, J. Braun, A. Kronenberg, S. Chadov, B. Balke, A. Gloskovskii, M. Kolbe, H.-J. Elmers, G. Schönhense, H. Ebert, C. Felser, and M. kläui, Nat. Commun. **5**, 3974 (2014).

[25] I. Galanakis, P. H. Dederichs, and N. Papanikolaou, Phys. Rev. B **66**, 174429 (2002).

[26] R. Y. Umetsu, K. Kobayashi, A. Fujita, K. Oikawa, R. Kainuma, K. Ishida, N. Endo, K. Fukamichi, and A. Sakuma, Phys. Rev. B **72**, 214412 (2005).

[27] I. Galanakis, P. Mavropoulos, and P. H. Dederichs, J. Phys. D: Appl. Phys. **39**, 765 (2006).

[28] V. Alijani, J. Winterlik, G. H. Fecher, S. S. Naghavi, and C. Felser, Phys. Rev. B **83**, 184428 (2011).

[29] Y. Venkateswara, D. Rani, K. Suresh, and A. Alam, J. Magn. Magn. Mater. **502**, 166536 (2020).

[30] R. Mahat, S. KC, U. Karki, J. Y. Law, V. Franco, I. Galanakis, A. Gupta, and P. LeClair, Phys. Rev. B **104**, 014430 (2021).

[31] V. K. Kushwaha, S. Kokado, S. Kasai, Y. Miura, T. Nakatani, R. Kumara, H. Tajiri, T. Furubayashi, K. Hono, and Y. Sakuraba, Phys. Rev. Mater. **6**, 064411 (2022).

[32] Y. Sakuraba, T. Miyakoshi, M. Oogane, Y. Ando, A. Sakuma, T. Miyazaki, and H. Kubota, Appl. Phys. Lett. **89**, 052508 (2006).

[33] S. Ueda, Y. Miura, Y. Fujita, and Y. Sakuraba, Phys. Rev. B **106**, 075101 (2022).

[34] G. H. Fecher, H. C. Kandpal, S. Wurmehl, C. Felser, and G. Schönhense, J. Appl. Phys. **99**, 08J106 (2006).

[35] H. C. Kandpal, G. H. Fecher, and C. Felser, J. Phys. D: Appl. Phys. **40**, 1507 (2007).

[36] J. Kübler, G. H. Fecher, and C. Felser, Phys. Rev. B **76**, 024414 (2007).

[37] T. Graf, C. Felser, and S. S. Parkin, Prog. Solid State Chem. **39**, 1 (2011).

[38] A. Husmann and L. J. Singh, Phys. Rev. B **73**, 172417 (2006).

[39] K. Manna, L. Muechler, T.-H. Kao, R. Stinshoff, Y. Zhang, J. Gooth, N. Kumar, G. Kreiner, K. Koepernik, R. Car, J. Kübler, G. H. Fecher, C. Shekhar, Y. Sun, and C. Felser, Phys. Rev. X **8**, 041045 (2018).

[40] B. Ernst, R. Sahoo, Y. Sun, J. Nayak, L. Muchler, A. K. Nayak, N. Kumar, J. Gayles, A. Markou, G. H. Fecher, and C. Felser, Phys. Rev. B **100**, 054445 (2019).

[41] S. Roy, R. Singha, A. Ghosh, A. Pariari, and P. Mandal, Phys. Rev. B **102**, 085147 (2020).

[42] P. Li, J. Koo, W. Ning, J. Li, L. Miao, L. Min, Y. Zhu, Y. Wang, N. Alem, C.-X. Liu, Z. Mao, and B. Yan, Nat. Commun. **11**, 1 (2020).

[43] G. K. Shukla, J. Sau, N. Shahi, A. K. Singh, M. Kumar, and S. Singh, Phys. Rev. B **104**, 195108 (2021).

[44] A. Sakai, Y. P. Mizuta, A. A. Nugroho, R. Sihombing, T. Koretsune, M.-T. Suzuki, N. Takemori, R. Ishii, D. Nishio-Hamane, R. Arita, P. Goswami, and S. Nakatsuji, Nat. Phys. **14**, 1119 (2018).

[45] K. Manna, Y. Sun, L. Muechler, J. Kübler, and C. Felser, Nat. Rev. Mater. **3**, 244 (2018).

[46] S. Picozzi, A. Continenza, and A. J. Freeman, Phys. Rev. B **66**, 094421 (2002).

[47] J.-C. Tung and G.-Y. Guo, New J. Phys. **15**, 033014 (2013).

[48] A. Okubo, R. Y. Umetsu, K. Kobayashi, R. Kainuma, and K. Ishida, Appl. Phys. Lett. **96**, 222507 (2010).

[49] Z. Wang, M. G. Vergniory, S. Kushwaha, M. Hirschberger, E. V. Chulkov, A. Ernst, N. P. Ong, R. J. Cava, and B. A. Bernevig, Phys. Rev. Lett. **117**, 236401 (2016).

[50] J. Noky, Y. Zhang, J. Gooth, C. Felser, and Y. Sun, npj Comput. Mater. **6**, 77 (2020).

[51] M. Obaida, K. Westerholt, and H. Zabel, Phys. Rev. B **84**, 184416 (2011).

[52] T. Kono, M. Kakoki, T. Yoshikawa, X. Wang, K. Goto, T. Muro, R. Y. Umetsu, and A. Kimura, Phys. Rev. Lett. **125**, 216403 (2020).

[53] See Supplemental Material at http://link.aps.org/supplemental/10.1103/PhysRevB.108.205108 for sample characterizations, field-dependent dc magnetization at different temperatures, and additional anomalous Hall effect analysis.

[54] S. Chatterjee, J. Sau, S. Ghosh, S. Samanta, B. Ghosh, M. Kumar, and K. Mandal, J. Phys.: Condens. Matter **35**, 035601 (2023).

[55] S. Ouardi, G. H. Fecher, B. Balke, A. Beleanu, X. Kozina, G. Stryganyuk, C. Felser, W. Klöß, H. Schrader, F. Bernardi, J. Morais, E. Ikenaga, Y. Yamashita, S. Ueda, and K. Kobayashi, Phys. Rev. B **84**, 155122 (2011).

[56] A. Markou, D. Kriegner, J. Gayles, L. Zhang, Y.-C. Chen, B. Ernst, Y.-H. Lai, W. Schnelle, Y.-H. Chu, Y. Sun, and C. Felser, Phys. Rev. B **100**, 054422 (2019).

[57] E. Vilanova Vidal, H. Schneider, and G. Jakob, Phys. Rev. B **83**, 174410 (2011).

[58] S. Chatterjee, J. Sau, S. Samanta, B. Ghosh, N. Kumar, M. Kumar, and K. Mandal, Phys. Rev. B **107**, 125138 (2023).

[59] R. Weiss and A. Marotta, J. Phys. Chem. Solids **9**, 302 (1959).

[60] S. Rathod, M. Malasi, A. Lakhani, and D. Kumar, Phys. Rev. Mater. **6**, 084202 (2022).

[61] Note: In the fitting of both Figs. 2(c) and 2(d) for Co$_2$MnGe, the Debye temperature (Θ_D) = 403 K has been considered, determined from the specific-heat measurement [55].

[62] B. Abderrahim, M. Ameri, D. Bensaid, Y. Azaz, B. Doumi, Y. Al-Douri, and F. Benzoudji, J. Supercond. Novel Magn. **29**, 277 (2016).

[63] N. Nagaosa, J. Sinova, S. Onoda, A. H. MacDonald, and N. P. Ong, Rev. Mod. Phys. **82**, 1539 (2010).

[64] R. Karplus and J. Luttinger, Phys. Rev. **95**, 1154 (1954).

[65] T. Jungwirth, Q. Niu, and A. H. MacDonald, Phys. Rev. Lett. **88**, 207208 (2002).

[66] N. Nagaosa, J. Phys. Soc. Jpn. **75**, 042001 (2006).

[67] J. Smit, Physica (Amsterdam) **21**, 877 (1955).

[68] J. Smit, Physica (Amsterdam) **24**, 39 (1958).

[69] P. Nozieres and C. Lewiner, J. Phys. (France) **34**, 901 (1973).

[70] S. Onoda, N. Sugimoto, and N. Nagaosa, Phys. Rev. Lett. **97**, 126602 (2006).

[71] Q. Wang, Y. Xu, R. Lou, Z. Liu, M. Li, Y. Huang, D. Shen, H. Weng, S. Wang, and H. Lei, Nat. Commun. **9**, 1 (2018).

[72] C. Zeng, Y. Yao, Q. Niu, and H. H. Weitering, Phys. Rev. Lett. **96**, 037204 (2006).

[73] Q. Wang, S. Sun, X. Zhang, F. Pang, and H. Lei, Phys. Rev. B **94**, 075135 (2016).